ELSEVIER

Chemical Geology 226 (2006) 115–133

CHEMICAL GEOLOGY
INCLUDING
ISOTOPE GEOSCIENCE

www.elsevier.com/locate/chemgeo

The isotopic composition of magnesium in mantle olivine: Records of depletion and metasomatism

N.J. Pearson [a,*], W.L. Griffin [a,b], O. Alard [a,c,d], Suzanne Y. O'Reilly [a]

[a] *GEMOC ARC National Key Centre, Department of Earth and Planetary Sciences, Macquarie University, NSW 2109, Australia*
[b] *CSIRO Exploration and Mining, North Ryde, NSW 2113, Australia*
[c] *Open University, Milton Keynes, MK7 6AA, UK*
[d] *Lab. De Tectonophysique, CNRS UMR 5568, ISTEEM, Université de Montpellier II, Pl. E. Bataillon, 34095 Montpellier Cedex05, France*

Accepted 5 September 2005

Abstract

We have investigated detailed Mg isotopic variations in the lithospheric mantle by analysing olivine in mantle-derived peridotite xenoliths and megacrysts. High-precision in situ analyses of $^{26}Mg/^{24}Mg$ and $^{25}Mg/^{24}Mg$ are made using a laser-ablation microprobe and MC-ICPMS. Measurements are done using a standard-sample bracketing technique with an in-house olivine standard. Replicate analyses of this standard give a precision of 0.20‰ (2sd) for $\delta^{26}Mg$ ($=[(^{26}Mg/^{24}Mg)_{sample}/(^{26}Mg/^{24}Mg)_{standard}-1]\times 1000$) and 0.12‰ (2sd) for $\delta^{25}Mg$. The analysed olivine grains represent the lithospheric mantle beneath Archean cratons (Siberia, Kaapvaal, Slave) and Phanerozoic fold belts (SE Australia).

Results from olivines show significant heterogeneity in the lithospheric mantle: $\delta^{26}Mg$ ranges from −3.01‰ to +1.03‰ and $\delta^{25}Mg$ from −1.59‰ to +0.51‰, relative to the magnesium isotopic standard DSM-3. There is a broad trend from lighter Mg isotopic compositions in depleted xenoliths from Archean mantle to heavier Mg in the less depleted Phanerozoic samples. Samples with petrographic evidence of refertilisation (including modal metasomatism) show large ranges in δMg values within samples. Sheared peridotite xenoliths from the Kaapvaal and Slave Cratons show a shift to higher δMg associated with the introduction of fluids with an 'asthenospheric' signature. Olivine in the least metasomatised peridotites from SE Australia has isotopically light Mg, whereas olivine in cryptically and modally metasomatised peridotites (amphibole ± apatite-bearing) becomes progressively heavier, both absolutely and relative to pyroxene and amphibole, with increasing degrees of metasomatism. The heterogeneity measured in individual samples suggests that Mg isotopic fractionations produced by processes of mantle metasomatism are preserved on the intra-grain scale, and the magnitude of the observed fractionations indicates that diffusion-related (kinetic) processes are important in controlling isotope fractionation at high temperatures. The in situ measurement of Mg isotopes provides a powerful new method for investigating processes in the mantle.
© 2005 Elsevier B.V. All rights reserved.

Keywords: Magnesium isotopes; Mantle olivine; Lithospheric mantle; Laser-ablation MC-ICPMS; Mantle metasomatism

1. Introduction

Recent developments in multi-collector inductively coupled plasma mass spectrometry (MC-ICPMS) have stimulated renewed interest in the variations in the isotopic composition of Mg in geological and biologi-

* Corresponding author: Fax: +61 2 9850 8349.
E-mail address: npearson@els.mq.edu.au (N.J. Pearson).

0009-2541/$ - see front matter © 2005 Elsevier B.V. All rights reserved.
doi:10.1016/j.chemgeo.2005.09.029

cal environments (Galy et al., 2000, 2001, 2002). The data obtained by Galy et al. using a Nu Plasma MC-ICPMS showed the precision to be more than an order of magnitude better than can be obtained using thermal ionization mass spectrometry. This marked improvement in precision allows the measurement of mass-dependent isotopic fractionations of Mg with a reproducibility of 30 to 60 ppm or better (Galy et al., 2001). These studies have demonstrated that the MC-ICPMS technique provides analyses with a standard deviation significantly smaller than the range of natural variation measured in terrestrial and extraterrestrial samples.

The application of Mg isotopes as a tracer in geochemical processes is still in its infancy and there are many areas to be explored. Previous studies have emphasized the role of volatilization and condensation reactions (Galy et al., 2000) and low-temperature fluid/rock interactions (Galy et al., 2002) as mechanisms for mass-dependent fractionation of Mg isotopes. Although mass-dependent fractionation is not predicted to be significant at high temperatures (Urey, 1947) the possibility exists that isotopic variations due to kinetic effects could occur in response to equilibrium partitioning fractionation or diffusion based processes (e.g. Richter et al., 1999). To date the Mg isotopic composition of the Earth's mantle has received little attention. Magnesium has three naturally occurring stable isotopes, ^{24}Mg (78.99%), ^{25}Mg (10.00%) and ^{26}Mg (11.01%). Galy et al. (2000) showed that the Mg isotopic abundances of terrestrial materials define a single mass fractionation trend, termed the Terrestrial Fractionation Curve (TFC), on a Mg three-isotope plot. The only published values for mantle materials are analyses of olivine and clinopyroxene from a mantle-derived peridotite (Young et al., 2002), which are within error of values for CI meteorites and the DSM-3 standard. On this basis, Galy et al. (2000) suggested that δ^{26}Mg = 0.0‰ (relative to the DSM-3 standard) is a reasonable estimate of the chondritic reservoir for Mg, and for the Earth's mantle. An important question is whether the Earth's lithospheric mantle is a uniform reservoir.

We have investigated this question by looking at the isotopic composition of Mg in different mantle domains to establish if it is uniform in space and time. If variations exist, can the processes that cause mass-dependent fractionation of Mg isotopes under mantle P–T conditions be identified? The approach adopted was to measure the isotopic composition of Mg in mantle-derived olivine using an in situ laser-ablation technique. The Mg-isotope composition of the olivine should reflect that of the bulk composition because olivine is typically the most abundant phase in mantle peridotites (modal range 60–100 vol.%; Griffin et al., 1999a, 2003b) and dominates the whole-rock budget for MgO. Olivine is also the most common host for 'enclosed' mantle sulfides, which can be dated using in situ Re–Os isotope techniques (Pearson et al., 2002; Griffin et al., 2002). Of interest here is whether Mg-isotope fractionation can provide information on the growth history of individual olivine grains.

The only previous detailed in situ study of the mass-dependent fractionation of Mg isotopes using laser-ablation MC-ICPMS was undertaken by Young et al. (2002). This work included the analysis of olivine, pyroxene and chondrules in the Allende meteorite and explored fractionation processes associated with alteration. The analytical method developed by Young et al. incorporated a sample-standard bracketing technique where the standard was a solution of the reference material SRM980. In this study a bracketing technique is also employed but an olivine is used as the standard. For this reason a detailed description of the analytical method and development of the olivine standard is given here.

2. Samples

2.1. Laser standards

Olivines from Almklovdalen, Norway (ALM-1 $Fo_{92.9 \pm 0.13}$, Ca 55 ± 2 ppm; ALM-2 $Fo_{93.2 \pm 0.15}$, Ca 117 ± 5 ppm) and San Carlos, Arizona, USA (SC-1; $Fo_{91.1 \pm 0.15}$; Ca 730 ± 20 ppm) initially were selected as potential laser standards. The Almklovdalen olivine occurs as large (several centimeters) gem-quality crystals in late hydrothermal veins within a large dunite body, and detailed electron microprobe analysis showed individual crystals to be chemically homogeneous. ALM-1 and ALM-2 are two individual crystals. The San Carlos material was available as smaller (to 5 mm) single gem-quality grains from disaggregated xenoliths of spinel peridotite. Individual grains are chemically homogeneous, but different grains may vary by 0.5% Fo, and SC-1 proved also to be less isotopically homogeneous than ALM-1 (see below). We therefore have used ALM-1 as our primary laser standard.

2.2. Xenoliths and xenocrysts

The olivine grains were analysed in a selection of mantle-derived peridotite xenoliths and megacrysts chosen to represent the lithospheric mantle beneath Archean cratons (Siberia, Kaapvaal, Slave) and Phanerozoic fold belts (south-eastern Australia).

2.2.1. Siberia

A suite of olivine xenocrysts from the Udachnaya kimberlite pipe was chosen for the study. The significance of the suite is that the olivines host sulfide inclusions which were the subject of an in situ Re–Os study by Griffin et al. (2002). The Udachnaya pipe is in the Archean Daldyn terrane of the Siberian Platform. The subcontinental lithospheric mantle (SCLM) beneath the Daldyn terrane is strongly depleted but shows a distinct layering (Griffin et al., 1996b, 1999a). The olivine xenocryst suite is interpreted to represent fragments of peridotites from a layer between 150 and 180 km deep, which is dominated by harzburgites and the unusual 'megacrystalline dunites'. The compositions of the olivines ($Fo_{92–93}$) fall within the range measured in xenoliths from this pipe.

2.2.2. Slave Craton

Xenoliths from the A154 kimberlite pipe, Lac de Gras were selected to represent the lithospheric mantle beneath the Slave Craton. This lithospheric section is characterized by a distinct layered structure with an upper ultra-depleted layer and a deeper more fertile layer with a sharp boundary at ~145 km (Griffin et al., 1998, 1999b). The suite of xenoliths has been described in detail by Pearson et al. (1999). Samples from both layers are incorporated in this study and cover the observed variety of rock types (spinel- and/or garnet-bearing harzburgites and lherzolites) and microstructures (coarse granular to 'sheared'). The microstructures range from coarse granular, through those that are partly recrystallized with the formation of olivine neoblasts, to the more strongly deformed mylonitic or 'sheared' types in which most of the olivine has recrystallized to finer grain sizes. The average composition of olivine in the upper layer is $Fo_{92.8}$ and in the lower layer is $Fo_{91.5}$. Compositions of individual samples are given in Table 3.

2.2.3. Kaapvaal Craton

Xenoliths representing the lithospheric mantle beneath the Kaapvaal Craton were sampled from kimberlites, including Letseng-le-Terai (samples LT98/-), pipes in the Kimberley area (BSF/-) and Jagersfontein (JGF-98/-). The locations of these kimberlite pipes in relation to terranes within the craton are discussed in Griffin et al. (2004). The xenoliths included in this study are spinel- and/or garnet-bearing harzburgites and lherzolites and they have been selected to study the effects of recrystallization and associated refertilisation/metasomatism (Griffin et al., 2003a, 2004). Compositions of individual samples are given in Table 3.

2.2.4. South-eastern Australia

Samples were chosen from the well-characterized suite of granular spinel lherzolite xenoliths from western Victoria (Griffin et al., 1984; O'Reilly and Griffin, 1988; Griffin et al., 1988; O'Reilly et al., 1991; Powell et al., 2004) and include both cryptically metasomatised ('dry') and modally metasomatised types. Modal metasomatism is indicated by the development of volatile-bearing phases such as apatite, amphibole, mica and carbonate. At least three distinct metasomatic events have affected the lithospheric mantle beneath western Victoria; Sr and Nd isotopic data from the peridotite xenoliths indicate that the oldest of these events may be Paleozoic, while the youngest occurred shortly before eruption (Griffin et al., 1988; Matsumoto et al., 2000). The average composition of the olivine in the suite is Fo_{89} (range Fo_{87} to Fo_{91}) and this is consistent with the fertile composition of this Phanerozoic lithosphere section compared with the more depleted Archean cratons.

3. Analytical methods

3.1. Sample preparation

3.1.1. Solutions

The international Mg isotopic standard SRM980 was used as the reference standard in the initial stages of this study. The Mg metal was dissolved in 2% HCl at room temperature and diluted in deionized water (Milli-Q 18.2 MΩ cm^{-1}). Following the results of the interlaboratory study that reported the heterogeneity of SRM980 (Galy et al., 2003) all subsequent solution measurements were made using DSM-3 as the reference standard. Cambridge-1 is a pure magnesium solution (Galy et al., 2003) and OU-Mg is an 'in-house' Mg reference prepared at the Open University. SPEX Mg is a high-purity ICP-MS elemental standard. We also have analysed Mg separated from the IAPSO sea water standard. Hand-picked fragments (100 mg) of the Almklovdalen and San Carlos olivines were digested using a conventional procedure. This involved digestion in 2 ml of double-distilled concentrated HNO_3 plus 2 ml of ARISTAR HF in a screw-top Savillex beaker. This was heated overnight at 120 °C and then evaporated slowly to incipient dryness at 150 °C. The previous two steps involving the $HF + HNO_3$ acid attack and evaporation to dryness were then repeated. Once dry 10 ml of 6 N HNO_3 was added and the beaker resealed, and heated overnight at 100 °C. Again the solution was

evaporated to incipient dryness. Ten milliliters of distilled 2% HNO_3 was added and the sealed beaker was heated at 100 °C until any residue was dissolved. All standards and sample solutions for analysis were prepared in 2% HNO_3 acid with concentrations of 50 to 200 ppb Mg.

3.1.2. Laser ablation

Pieces (~20 × 10 mm in section) of two single olivine crystals from Almkovdalen were prepared as standards. Four individual olivine grains (~5 × 5 mm in section) from San Carlos xenoliths were mounted in a 25 mm diameter polished block. All of the xenoliths were prepared as polished thick sections (100 to 150 μm) and the xenocrysts as polished blocks.

3.2. Laser ablation

In situ analysis was performed using either a New Wave Merchantek LUV266 or LUV213 Nd:YAG laser-ablation system attached to a Nu Plasma MC-ICPMS. Samples were ablated in He and the He-sample aerosol was then mixed with Ar before introduction into the plasma. Typical laser operating conditions for both systems were a frequency of 5 Hz and energy of ~0.1 mJ giving a spot size of ~30 to 50 μm and a typical total Mg beam size of 5–9 V.

3.3. Mass spectrometry

Mg-isotope ratios for standard solutions and all in situ analyses of olivine were measured using a Nu Plasma MC-ICPMS (NU005). The standard solutions were also analysed on a Nu Plasma HR MC-ICPMS (NU034). Operating conditions for both mass spectrometers are similar to those described by Galy et al. (2001). The Nu Plasma has a fixed collector array of 12 Faraday collectors and the variable dispersion ion optics are used to direct the Mg isotopes into the axial (^{25}Mg) and the two outermost Faradays (^{24}Mg and ^{26}Mg). Measurements on NU034 were conducted with the low-resolution defining slit, giving the same mass resolution as NU005. The mass spectrometer was tuned to give maximum sensitivity. Solution concentrations and laser operating conditions were adjusted to bring ^{24}Mg signals into the working range of the Faraday cups i.e. <10 V (or 1E−10 A).

3.3.1. Solution analyses

Two different desolvating nebuliser systems were used to introduce the solutions into the MC-ICPMS: a CETAC MCN 6000 was used on NU005 and a Nu Instruments DSN100 on NU034. Nitrogen was not used on either desolvating system. The main reason for using the desolvation units was to reduce the introduction of H_2O, CO_2, O_2 and N_2 into the plasma with the specific aim of minimizing hydride formation. The main difference between the MCN6000 and DSN100 relevant to this study is the difference in uptake rates of the two systems, which are approximately 60 and 100 μl/min, respectively. The higher consumption of the DSN100 and the overall higher sensitivity of NU034 necessitated a 50% dilution of the Mg standard solutions that were run on NU005.

The analysis routine incorporates peak centering on ^{24}Mg at the start of analysis (rather than for each block) followed by 60 measurements in 3 blocks of 20 cycles of 10 s, with 30 s zero measurements at the start of each block. Faraday zeros are measured at half-mass offsets and with ESA deflect. The washout routine involves aspirating first with Milli-Q H_2O, followed by 10% HNO_3, then by 3 sequential washes in 2% HNO_3 for 2 min each.

Galy et al. (2001) estimated the residual electronic noise after background correction to be $\sim 7 \times 10^{-17}$ A. The ^{24}Mg signal intensity measured for 2% HNO_3 is typically less than 0.1 mV over sessions of several days and this would contribute a systematic bias on δ^{26}Mg < 0.02‰. While the desolvation units reduce the potential interferences from H, N and O, the residual signal on ^{24}Mg can most likely be attributed to the ^{12}C dimer produced by air entrainment in the plasma.

3.3.2. Laser ablation

All measurements were done using the time-resolved acquisition mode of the Nu Plasma software. An on-mass gas background was collected for ~30 s and typical ablation times were 120–150 s. Signal intensities are recorded every 0.2 s and the time-integrated signal is treated as a total of 40 measurements for the calculation of internal precision.

4. Results

4.1. Solution analyses

The results for the solution analyses of SRM980, DSM-3, Cambridge-1, SPEX Mg, OU-Mg, ALM-1, ALM-2 and SC-1 are presented in Table 1. Mg-isotope compositions of solutions measured on NU005 are expressed as per mil (‰) deviation from the isotopic

Table 1
Magnesium isotopic composition of reference materials, commercial reagents and olivine standards

Standard		n	δ^{26}Mg (‰)	±2sd	δ^{25}Mg (‰)	±2sd	Ref.
Analyses measured on NU005 (Jan–July 2002); normalised to SRM980-MU							
SRM980-MU	Mg metal	68	0.00	0.13	0.00	0.11	
SPEX Mg	Mg solution	48	−1.80	0.18	−0.93	0.13	
ALM-1	Olivine	30	2.71	0.19	1.40	0.10	
ALM-2	Olivine	15	2.73	0.26	1.41	0.14	
SC-1	Olivine	10	2.99	0.25	1.54	0.18	
Analyses normalised to DSM-3							
DSM-3	Mg solution	129	0.00	0.34	0.00	0.16	1b
SRM980-MU	Mg metal	15	−3.63	0.18	−1.92	0.10	1b
Cambridge-1	Mg solution	69	−2.57	0.13	−1.34	0.04	1b
Cambridge-1	Mg solution	35	−2.58	0.14	−1.33	0.07	2
Cambridge-1	Mg solution	28	−2.63	0.19	−1.35	0.09	3
Cambridge-1	Mg solution	6	−2.62	0.12	−1.35	0.07	4
OU	Mg solution	47	−2.80	0.12	−1.45	0.06	1b
OU	Mg solution	31	−2.83	0.11	−1.46	0.05	3
OU	Mg solution	4	−2.77	0.12	−1.44	0.08	4
IAPSO	Sea water	8	−0.75	0.13	−0.39	0.07	1b
IAPSO	Sea water	5	−0.83	0.05	−0.40	0.04	3
North Atlantic	Sea water	4	−0.83	0.11	−0.42	0.09	5
IAPSO	Sea water	3	−0.55	0.02	−0.30	0.08	4
Worldwide	Sea water	14	−0.82	0.10	n.g.	–	6
ALM-1	Olivine	6	−0.92	0.09	−0.45	0.05	1b
ALM-1	Olivine	30	−0.92	0.26	−0.52	0.14	1a
SC-1	Olivine	6	−0.58	0.15	−0.28	0.10	1b
SC-1	Olivine	10	−0.64	0.31	−0.38	0.20	1a

1a: This study, analyses measured on NU005 (Jan–July 2004) relative to SRM980-MU normalised to DSM-3 using δ^{26}Mg (SRM980-MU)$_{DSM\text{-}3}$ = −3.63 ± 0.18 and δ^{25}Mg(SRM980-MU)$_{DSM\text{-}3}$ = −1.92 ± 0.10, errors are propagated through.
1b: This study, analyses measured on NU034 (Oct–Nov 2004).
2: Data from Galy et al. (2003).
3: Analyses performed at the Open University (NU002-2004).
4: Data from Wombacher et al. (2004).
5: Data from Chang et al. (2003), analysed relative to NIST SRM980-Oxford converted relative to DSM-3 using δ^{26}Mg (SRM980-*Oxf*)$_{DSM\text{-}3}$ = −3.40 ± 0.13 and δ^{25}Mg(SRM980-*Oxf*)$_{DSM\text{-}3}$ = −1.74 ± 0.07 (Galy et al., 2003).
6: Data from Carder et al. (2004) obtained on sea water from the Atlantic, Pacific, Indian Oceans and the Mediterranean, Red and Dead Seas.

composition of SRM980. The definitions of $\delta^{25}Mg_{SRM}$ and $\delta^{26}Mg_{SRM}$ are:

$$\delta^{n}\mathrm{Mg}_{\mathrm{SRM980}} = \left[\left({}^{n}\mathrm{Mg}/{}^{24}\mathrm{Mg}\right)_{\mathrm{sample}} / \left({}^{n}\mathrm{Mg}/{}^{24}\mathrm{Mg}\right)_{\mathrm{SRM980}} - 1\right] \times 1000$$

where n refers to either 25 or 26.

Mg-isotope compositions of solutions measured on NU034 are expressed as per mil (‰) deviation from the isotopic composition of DSM-3. The definitions of $\delta^{25}Mg_{DSM\text{-}3}$ and $\delta^{26}Mg_{DSM\text{-}3}$ are:

$$\delta^{n}\mathrm{Mg}_{\mathrm{DSM-3}} = \left[\left({}^{n}\mathrm{Mg}/{}^{24}\mathrm{Mg}\right)_{\mathrm{sample}} / \left({}^{n}\mathrm{Mg}/{}^{24}\mathrm{Mg}\right)_{\mathrm{DSM-3}} - 1\right] \times 1000$$

where n refers to either 25 or 26.

A standard-sampling bracketing technique was used to minimize the effects of drift in instrument mass bias. Uncorrected, these variations may be up to 0.6‰ in a day and 4‰ between days. The reproducibility of SRM980 measured as an unknown on NU005 and corrected for mass bias variation with time is ±0.13 (2sd) for $\delta^{26}Mg_{SRM980}$ and ±0.11 (2sd) for $\delta^{25}Mg_{SRM980}$ (Fig. 1). The reproducibility of DSM-3 measured as an unknown on NU034 and corrected for mass bias variation with time is ±0.34 (2sd) $\delta^{26}Mg_{DSM\text{-}3}$ and ±0.16 (2sd) for $\delta^{25}Mg_{DSM\text{-}3}$ (Fig. 2).

Relative to DSM-3, GEMOC SRM980 has $\delta^{26}Mg_{DSM\text{-}3}$ = −3.63 ± 0.18 and $\delta^{25}Mg_{DSM\text{-}3}$ = −1.92 ± 0.10, and is similar in composition to the Oxford SRM980 ($\delta^{26}Mg_{DSM\text{-}3}$ = −3.40 ± 0.13; $\delta^{25}Mg_{DSM\text{-}3}$ = −1.74 ± 0.07; Galy et al., 2003). Analyses of the Cambridge-1, OU-Mg and IAPSO sea water solutions all give mean values identical within uncertainties to data obtained in other laboratories (Table 1). All three olivine solutions have significantly heavier isotopic compositions than SRM980, OU and SPEX Mg.

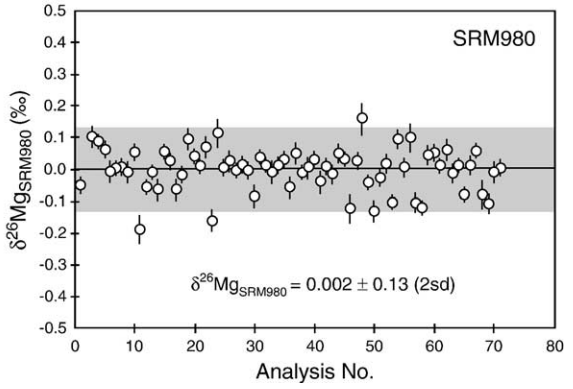

Fig. 1. Reproducibility of δ^{26}Mg measurements of SRM980 solution made over a 6-month period on NU005. The shaded area corresponds to the 2σ of the complete data set. Error bars on individual measurements are 1 standard error.

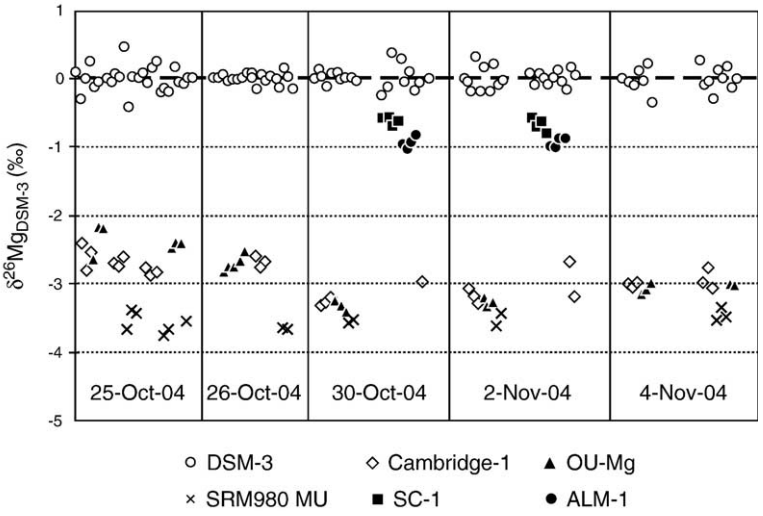

Fig. 2. Reproducibility of δ^{26}Mg measurements of DSM-3 solution over a period of 10 days on NU034. Also shown are the within-session and day-to-day variations in SRM980, Cambridge-1, OU-Mg, SC-1 and ALM-1 solutions.

The two Almklovdalen olivine solutions (ALM-1 and ALM-2) are identical within analytical uncertainties ($\delta^{26}Mg_{SRM980} = 2.71 \pm 0.19$ and 2.73 ± 0.26, respectively); SC-1 is slightly heavier ($\delta^{26}Mg_{SRM980} = 2.99 \pm 0.25$) but within analytical uncertainty. These results are confirmed by the measurements undertaken on NU034 using DSM-3 as the reference standard (Table 1). The compositions of ALM-1 ($\delta^{26}Mg_{DSM\text{-}3} = -0.92 \pm 0.09$, $\delta^{25}Mg_{DSM\text{-}3} = -0.45 \pm 0.05$) and SC-1 ($\delta^{26}Mg_{DSM\text{-}3} = -0.58 \pm 0.15$, $\delta^{25}Mg_{DSM\text{-}3} = -0.28 \pm 0.10$) are both lighter than DSM-3. The results obtained in this study for the Cambridge-1 solution ($\delta^{26}Mg_{DSM\text{-}3} = -2.57 \pm 0.13$, $\delta^{25}Mg_{DSM\text{-}3} = -1.34 \pm 0.04$) are identical to the values reported by Galy et al. (2003); ($\delta^{26}Mg_{DSM\text{-}3} = -2.58 \pm 0.14$, $\delta^{25}Mg_{DSM\text{-}3} = -1.33 \pm 0.07$). The composition of the SPEX Mg ($\delta^{26}Mg_{SRM} = -1.80 \pm 0.18$ relative to SRM980) is of interest because it is significantly lower than SRM980, but attempts to trace the source of the Mg have been unsuccessful. The value obtained for δ^{26}Mg for the OU-Mg standard ($\delta^{26}Mg_{DSM\text{-}3} = -2.80 \pm 0.12$) is identical to the average value determined at the Open University (O. Alard, unpublished data), and the value reported by Wombacher et al. (2004).

The results of the solution analyses obtained are shown in the three-isotope plot of the Mg-isotope ratios (Fig. 3). The slope of the line of best fit through the solution analyses is 0.5165 ± 0.0005 and is within uncertainty of the value obtained by Galy et al. (2001) for the TFC (slope $= 0.5163 \pm 0.0004$).

The relationship between $^{25}Mg/^{24}Mg$ and $^{26}Mg/^{24}Mg$ can also be used to define the instrumental mass-dependent fractionation. The definitions below follow the notation of Galy et al. (2001):

$$\alpha^{25}_{inst} = \left(^{25}Mg/^{24}Mg\right)_{measured} / \left(^{25}Mg/^{24}Mg\right)_{true}$$

$$\alpha^{26}_{inst} = \left(^{26}Mg/^{24}Mg\right)_{measured} / \left(^{26}Mg/^{24}Mg\right)_{true}$$

The theoretical relationship between these two parameters is given by

$$\alpha^{25}_{inst} = \left(\alpha^{26}_{inst}\right)\wedge\beta$$

where β is the mass fractionation coefficient.

Measurements of α_{inst} on the GEMOC Nu Plasma NU005 give a value for $\beta = 0.5187 \pm 0.0005$ (Fig. 4). This value is within error of the value ($\beta = 0.5180 \pm 0.0004$)

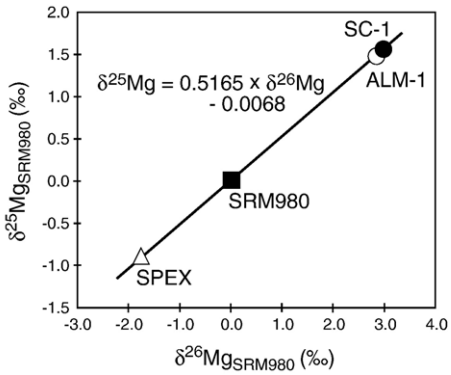

Fig. 3. Magnesium three-isotope plot (relative to SRM980 Mg standard) of SPEX Mg, ALM-1 (Almklovdalen olivine) and SC-1 (San Carlos olivine) solutions.

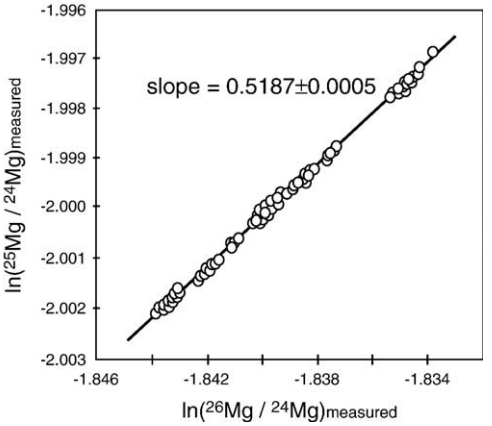

Fig. 4. Three-isotope plot of natural logarithm of Mg-isotope ratios of SRM980. The slope of the line gives the value for β, and defines the relationship between the instrumental mass-dependent fractionation for the $^{25}Mg/^{24}Mg$ (α^{25}_{inst}) and $^{26}Mg/^{24}Mg$ (α^{26}_{inst}) ratios.

obtained by Galy et al. (2001), who state that because the value for β is closer to the theoretical value for thermodynamic equilibrium (0.5210) than for kinetic equilibrium (0.5105), isotopic fractionation in the MC-ICPMS can be attributed to near-equilibrium processes.

The solutions for the ALM-1 and SC-1 olivines were not processed to separate the magnesium; this was done to provide an analogue as close as possible to the laser-ablation situation. The solutions were scanned on an Agilent 7500 ICPMS and as expected Fe was the only other element present at a significant abundance. In order to assess the effect of Fe on mass fractionation a series of solutions was prepared in which SRM980 was spiked with high-purity Fe (IRMM14) to give a range of synthetic olivine compositions (Fo_{90}, Fo_{80}, Fo_{50}). The solutions were analysed on NU005 over a period of 18 months and once on NU034 (Fig. 5). The results show no systematic relationship between Fe : Mg and the SRM980 Mg-isotope ratio, and all measurements are within uncertainty limits (± 0.13, 2sd) of the long-term average value for SRM980.

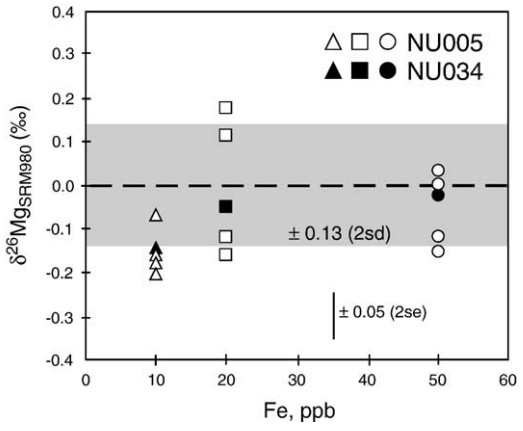

Fig. 5. Deviations in $\delta^{26}Mg$ values of SRM980 as a function of added Fe (IRMM14). Measurements of the iron-spiked solutions obtained on NU005 are shown as open symbols and those obtained on NU034 are shown as closed symbols. The shaded area corresponds to the 2σ of the unspiked SRM980 in Fig. 1.

Table 2
Mg isotopic composition of olivine standards by laser ablation

Standard		n	$\delta^{26}Mg_{ALM-1}$ (‰)	± 2sd	$\delta^{25}Mg_{ALM-1}$ (‰)	± 2sd
ALM-1	Olivine	109	0.02	0.20	0.01	0.12
ALM-2	Olivine	10	0.12	0.18	0.06	0.08
SC-1	Olivine	37	0.38	0.37	0.20	0.18

Measured relative to ALM-1 and converted to DSM-3 scale using solution values $\delta^{26}Mg = -0.92$ and $\delta^{25}Mg = -0.45$.

4.2. Laser ablation

4.2.1. Evaluation of ALM-1, ALM-2 and SC-1

ALM-1, ALM-2 and SC-1 were analysed as 'unknowns' within runs using a standard-sample bracketing technique with either ALM-1 or SC-1 as the reference standard. The results are presented in Table 2. The data obtained by laser ablation are consistent with the solution results, with SC-1 having a higher $\delta^{26}Mg$ than ALM-1 and ALM-2. The $\delta^{26}Mg$ values for ALM-1 and ALM-2 are within uncertainty limits (2sd) of each other. The variation of laser operating conditions, total Mg beam intensity and count times gave a typical internal precision $< \pm 0.000010$ (2se) on both ALM-1 and SC-1. The long-term reproducibility of the $\delta^{26}Mg$ measurement on ALM-1 is shown in Fig. 6. Replicate analyses of the Almklovdalen olivine indicate a precision of 0.20‰ (2σ) for $\delta^{26}Mg$ and 0.12‰ (2σ)

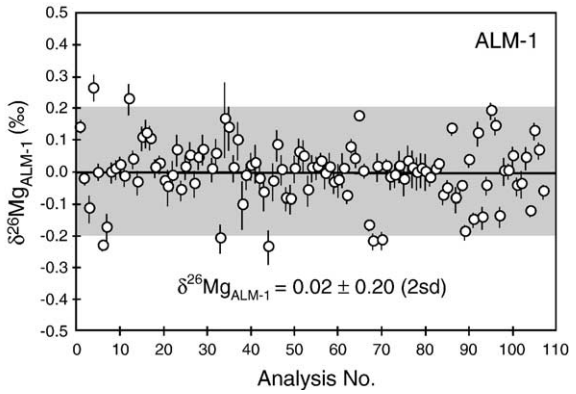

Fig. 6. Reproducibility of $\delta^{26}Mg$ measurements of ALM-1 by laser ablation. The shaded area corresponds to the 2σ of the complete data set. Error bars on individual measurements are 1 standard error.

for δ^{25}Mg. The reproducibility of the analyses of SC-1 is not as good as for ALM-1, with a precision of 0.37‰ (2σ) for δ^{26}Mg and 0.20‰ (2σ) for δ^{25}Mg (Fig. 7), even though all analyses reported here were made on a single grain. This might indicate some isotopic inhomogeneity in SC-1, and ALM-1 was chosen as the laser reference standard for the analyses of the sample olivines.

4.2.2. Instrument fractionation

A three-isotope plot of measured α_{inst} for ALM-1 gives a $\beta = 0.5145 \pm 0.0008$ (Fig. 8). This is lower than the solution value and not within the uncertainty range, indicating that there is an apparent difference in instrumental mass-dependent fractionation for laser ablation. This does not necessarily mean that the difference in β values is due to a laser-induced fractionation. The precision obtained on individual measurements (typically better than 20 ppm) indicates that mass bias is stable over the period of the ablation (3 min). A plot of signal intensity and ^{26}Mg/^{24}Mg ratio versus time for a typical laser analysis of ALM-1 is shown in Fig. 9. Although the signal intensity decreases with time, the ratio remains unchanged; this is a clear indication that laser-induced mass fractionation is not significant or at least is time-independent over the duration of a typical ablation.

Freedman (2002) has suggested that the two main contributions to mass fractionation occur in the plasma and the interface region. One possibility is that the difference in β values for solution and laser ablation might be due to the fact that desolvation systems do not produce completely dry aerosols and this difference in fluid content might affect fractionation processes in the plasma. Particle-size distribution is also considered to be a significant factor responsible for isotopic fractionation in laser ablation; the incomplete ionization of larger particles in the plasma results in preferential transmission of lighter isotopes (Jackson and Gunther, 2003). This could be considered as a laser-induced phenomenon, but the fractionation is being produced in the plasma rather than at the site of ablation.

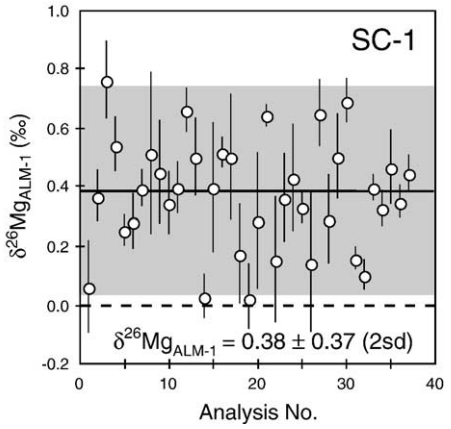

Fig. 7. Reproducibility of δ^{26}Mg measurements of SC-1 by laser ablation. The shaded area corresponds to the 2σ of the complete data set. Error bars on individual measurements are 1 standard error.

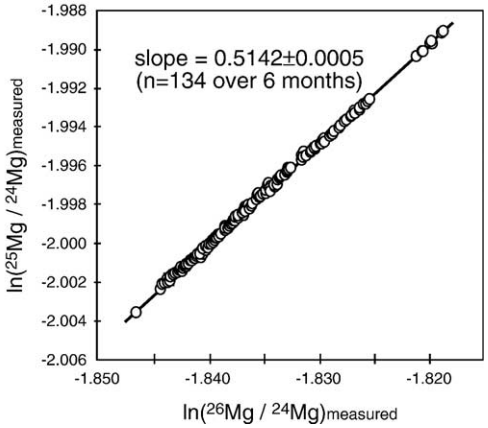

Fig. 8. Three-isotope plot of natural logarithm of Mg-isotope ratios of ALM-1. The slope of the line gives the value for B, and defines the relationship between the instrumental mass-dependent fractionation for the ^{25}Mg/^{24}Mg (α^{25}_{inst}) and ^{26}Mg/^{24}Mg (α^{26}_{inst}) ratios.

The data used to determine the β value for ALM-1 were obtained using both 213 and 266 nm Nd:YAG lasers. The relatively low uncertainty on β suggests that there is no evident variation in the fundamental instrumental mass-dependent fractionation that can be related to laser wavelength. On closer inspection, different values of β are determined for the measurements using the 266 nm laser ($\beta = 0.5163 \pm 0.14$) and the 213 nm laser ($\beta = 0.5136 \pm 0.20$), but the two values are within uncertainty of each other. Further experiments under controlled conditions need to be performed to investigate the possible relationship between β and laser wavelength. An alternative explanation is that the introduction of He into the plasma with the ablated sample changes the pressure in the interface region and causes the observed lower β values for the laser analyses compared with the β value for the solution measurements. A systematic shift in exponential fractionation coefficients for Hf isotopes is observed when ablation is done in a He atmosphere as opposed to Ar (authors' unpublished data). However, in the case of Hf there is no discernible change in slope for β between solution and laser ablation. This could be a function of atomic number but clearly the addition of He does change mass fractionation and in the case of Mg isotopes, processes in the interface region therefore might

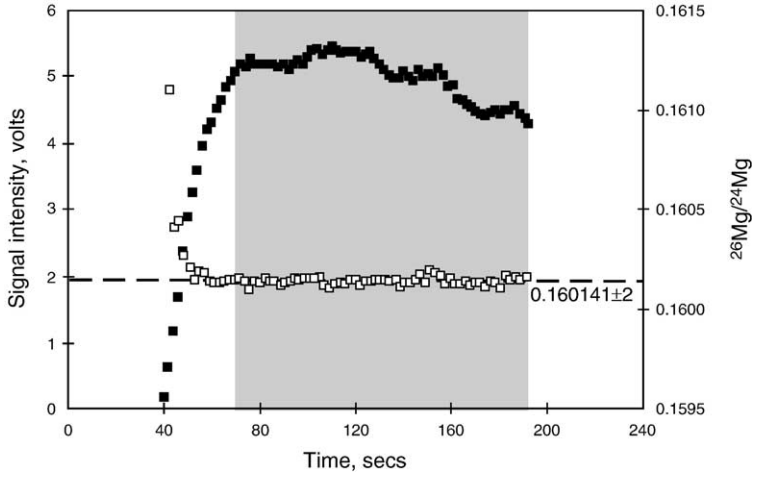

Fig. 9. A plot of total signal intensity (volts) and $^{26}Mg/^{24}Mg$ versus time for a typical laser-ablation analysis of ALM-1.

have a more significant effect on the instrumental mass fractionation.

4.3. Xenoliths and xenocrysts

All in situ measurements were made using a standard-sample bracketing technique with ALM-1 olivine as the standard. The standard was mounted in the cell at all times. δMg values were then converted to the equivalent delta values relative to DSM-3 using the following expression:

$$\delta^n Mg_{DSM-3} = \delta^n Mg_{ALM-1} + \delta^n Mg_{ALM-1/DSM-3} + 0.001\delta^n Mg_{ALM-1} \times \delta^n Mg_{ALM-1/DSM-3}$$

where $n=25$ or 26; $\delta^n Mg_{ALM\text{-}1} = [(^nMg/^{24}Mg)_{sample}/(^nMg/^{24}Mg)_{ALM\text{-}1} - 1] \times 1000$ is the measured value for the unknown relative to ALM-1; and $\delta^n Mg_{ALM\text{-}1/DSM\text{-}3}$ is the solution value of ALM-1 relative to the DSM-3 scale. The values for $\delta^n Mg_{ALM\text{-}1/DSM\text{-}3}$ are given in Table 2.

The results for the olivine samples presented in Table 3 show that there are significant variations in δ^{26}Mg and δ^{25}Mg in the lithospheric mantle. The overall range determined for the samples analysed in this study is from −3.01‰ to 1.03‰ for $\delta^{26}Mg_{DSM\text{-}3}$ and −1.59‰ to 0.51‰ for $\delta^{25}Mg_{DSM\text{-}3}$ (Fig. 10). While these absolute values are dependent on the composition of the DSM-3 used in this study, the relative variations should be unaffected. There is a broad trend from lighter Mg-isotope compositions in more depleted Archean samples to heavier compositions in the Phanerozoic samples from south-eastern Australia (Fig. 11), although there is considerable overlap between suites. The median value for $\delta^{26}Mg_{DSM\text{-}3}$ is −0.79‰ for the Siberian xenocrysts and the porphyroclasts in the Slave and Kaapvaal xenoliths, and −0.45‰ for south-eastern Australia. Of greater significance are the variations measured in single grains and from grain to grain within samples. In all cases where cores and rims were measured, the within-grain variation indicates a core-to-rim increase in δMg. The largest difference is recorded in one of the Siberian xenocrysts, ZS1, which has a range in $\delta^{26}Mg_{DSM\text{-}3}$ from −2.41‰ to −0.64‰. More typically the variation is <0.5‰, but this is still significant when compared to the external precision (±0.20‰, 2sd) obtained on ALM-1.

Many of the mildly to strongly deformed xenoliths studied show inter-granular isotopic variations that can be related to microstructural context. The garnet peridotites from Slave and Kaapvaal show a systematic increase of δ^{26}Mg with decreasing grain size. The relict coarse porphyroclasts have the lightest isotopic compositions and the fine-grained neoblasts the heaviest, with overall differences of up to 1.2‰ in single samples. This relationship (Fig. 12) has been found in both lherzolites and harzburgites and is most pronounced for adjacent porphyroclast–neoblast pairs.

The overall range for the six spinel lherzolites from south-eastern Australia is 3.3‰ δ^{26}Mg. One of the most significant aspects of the results is the consistent shift to heavier compositions in the strongly modally metasomatised samples (Fig. 13); these samples have limited inter-grain variation. The ‘dry’ or cryptically metasomatised samples, besides having the lightest compositions in the suite, also show greater within-sample variations. The range of values for $\delta^{26}Mg_{DSM\text{-}3}$ in

Table 3
Magnesium isotopic composition of olivine

Sample no.	Rock type	Notes	Fo	$\delta^{26}Mg_{ALM-1}$				$\delta^{25}Mg_{ALM-1}$				$\delta^{26}Mg_{DSM-3}$			$\delta^{25}Mg_{DSM-3}$		
				Average (‰)	sd	Min	Max	Average (‰)	sd	Min	Max	Average (‰)	Min	Max	Average (‰)	Min	Max
South-eastern Australia																	
DR9894	Sp lherzolite	D	88.3	−0.51	0.82	−1.98	0.65	−0.21	0.41	−0.93	0.31	−1.43	−2.89	−0.28	−0.66	−1.38	−0.14
DR9708	Sp lherzolite	(A)	90.3	−1.05	0.81	−2.09	0.25	−0.56	0.43	−1.14	0.15	−1.97	−3.01	−0.67	−1.01	−1.59	−0.31
SGN-1	Sp lherzolite	A	92.0	−0.27	0.16	−0.40	0.01	−0.14	0.10	−0.23	0.01	−1.19	−1.32	−0.91	−0.59	−0.68	−0.44
BM650	Sp lherzolite	AAp	87.5	−0.09	0.48	−1.06	0.55	−0.07	0.26	−0.58	0.29	−1.01	−1.98	−0.37	−0.52	−1.03	−0.16
BM901	Sp lherzolite	AAp	87.2	0.41	0.38	−0.01	1.03	0.20	0.21	−0.06	0.51	−0.51	−0.93	0.11	−0.25	−0.51	0.06
BM655	Sp lherzolite	AAp	89.8	0.67	0.27	0.24	1.21	0.35	0.14	0.13	0.67	−0.26	−0.68	0.29	−0.10	−0.32	0.22
D = dry; (A) = rare amphibole; A = amphibole; Ap = apatite																	
Slave Craton																	
vr40305	Sp–grt lherzolite	Coarse	92.4	−0.32	0.28	−0.59	0.14	−0.20	0.12	−0.33	−0.01	−1.24	−1.51	−0.78	−0.65	−0.78	−0.46
vr19764perg3	Sp–grt lherzolite	Coarse	92.8	0.45	0.36	0.07	1.11	0.28	0.20	0.08	0.61	−0.47	−0.85	0.19	−0.17	−0.37	0.16
vr09364a	Grt harzburgite		92.4	0.75	0.71	−0.32	1.85	0.41	0.36	−0.13	0.96	−0.17	−1.23	0.92	−0.04	−0.58	0.51
vr09361	Grt harzburgite		91.5	1.02	0.28	0.74	1.42	0.53	0.15	0.35	0.73	0.10	−0.18	0.50	0.08	−0.10	0.28
vr50855a	Grt harzburgite		92.4	0.35	0.58	−0.98	1.65	0.19	0.30	−0.50	0.86	−0.57	−1.90	0.73	−0.26	−0.95	0.41
vr50879	Grt harzburgite		90.4	0.61	0.47	0.00	1.61	0.27	0.25	−0.05	0.81	−0.32	−0.92	0.69	−0.18	−0.50	0.36
vr40332a	Grt lherzolite	Sheared	91.9	−0.03	0.34	−0.60	0.58	−0.05	0.18	−0.41	0.33	−0.95	−1.52	−0.34	−0.50	−0.86	−0.12
vr50886	Grt lherzolite	Sheared	89.9	−0.21	0.39	−1.25	0.28	−0.08	0.20	−0.61	0.19	−1.13	−2.17	−0.64	−0.53	−1.06	−0.26
Kaapvaal Craton																	
LTS98-17	Grt lherzolite	Sheared	89.7	0.82	0.66	−0.75	1.95	0.37	0.35	−0.56	0.96	−0.10	−1.67	1.03	−0.08	−1.01	0.51
JGF98-2	Grt harzburgite	Sheared	90.2	0.39	0.29	−0.09	0.58	0.21	0.19	−0.10	0.36	−0.53	−1.01	−0.34	−0.24	−0.55	−0.09
JGF98-3	Grt lherzolite	Sheared	90.5	0.50	0.40	0.01	0.96	0.27	0.22	−0.01	0.48	−0.42	−0.91	0.04	−0.18	−0.46	0.03
BSF98-23	Grt lherzolite	Coarse	91.8	0.32	0.40	−0.17	0.85	0.17	0.24	−0.08	0.51	−0.60	−1.09	−0.07	−0.28	−0.53	0.06
Siberian Craton																	
ZS1-1	Xenocryst		91.5	−0.77	0.61	−1.49	0.29	−0.37	0.32	−0.74	0.22	−1.69	−2.41	−0.64	−0.82	−1.19	−0.23
ZS2-1	Xenocryst		92.4	−0.06	0.39	−0.62	0.61	−0.05	0.19	−0.31	0.30	−0.98	−1.54	−0.31	−0.50	−0.76	−0.15
ZS3-3	Xenocryst		93.3	−0.22	0.22	−0.58	0.02	−0.13	0.13	−0.34	0.02	−1.14	−1.50	−0.90	−0.58	−0.79	−0.43
ZS4-3	Xenocryst		92.5	0.05	0.28	−0.29	0.42	0.03	0.15	−0.15	0.23	−0.87	−1.21	−0.50	−0.42	−0.60	−0.22
ZS9-1	Xenocryst		92.6	0.22	0.41	−0.12	0.68	0.07	0.20	−0.11	0.29	−0.70	−1.04	−0.24	−0.38	−0.56	−0.16
ZS10-1	Xenocryst		92.5	0.21	0.35	−0.38	0.83	0.11	0.19	−0.22	0.44	−0.71	−1.30	−0.09	−0.34	−0.67	−0.01
ZS11-3	Xenocryst		91.6	−0.45	0.15	−0.62	−0.35	−0.24	0.04	−0.29	−0.22	−1.37	−1.54	−1.27	−0.69	−0.74	−0.67
ZS13-3	Xenocryst		91.6	0.18	0.07	0.11	0.25	0.12	0.01	0.11	0.13	−0.74	−0.81	−0.67	−0.33	−0.34	−0.32
ZS14-1	Xenocryst		91.8	0.13	0.51	−0.46	0.44	−0.03	0.31	−0.39	0.18	−0.79	−1.38	−0.48	−0.48	−0.84	−0.27
ZS53-2	Xenocryst		92.4	−1.32	0.19	−1.54	−1.21	−0.67	0.09	−0.77	−0.60	−2.24	−2.46	−2.13	−1.12	−1.22	−1.05
ZS54-1	Xenocryst		93.9	0.06	0.33	−0.29	0.38	0.04	0.16	−0.13	0.19	−0.86	−1.21	−0.54	−0.41	−0.58	−0.26
ZS55-1	Xenocryst		94.5	−0.05	0.43	−0.69	0.26	0.00	0.20	−0.30	0.13	−0.97	−1.61	−0.66	−0.45	−0.75	−0.32
ZS56-2	Xenocryst		92.9	−0.13	0.17	−0.33	−0.02	−0.10	0.12	−0.23	−0.02	−1.05	−1.25	−0.94	−0.54	−0.68	−0.47

δMg values are shown as measured against ALM-1 and converted to the DSM-3 scale as described in the text.

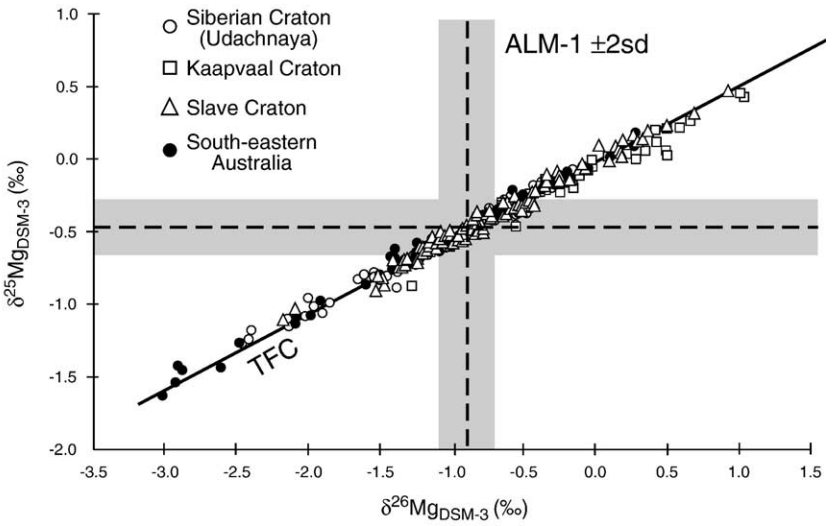

Fig. 10. Magnesium three-isotope plot (relative to DSM-3) of laser-ablation analyses of olivine from peridotite xenoliths and megacrysts from the lithospheric mantle. The line labeled TFC is the Terrestrial Fractionation Curve (TFC) from Galy et al. (2000).

DR9894 is −2.89‰ to −0.28‰ and in DR9708 it is −3.01‰ to −0.67‰. In both samples the heaviest compositions are similar to those obtained in the samples with abundant amphibole.

5. Discussion

5.1. Analytical issues

Matrix effects can be considered as spectral and non-spectral (Albarede and Beard, 2004), and are different for solution and laser analysis. There are no elemental isobaric interferences on the three Mg isotopes but there are several potential molecular interfering species, including $^{48}Ti^{++}$, $^{50}Ti^{++}$, $^{48}Ca^{++}$, $^{50}Cr^{++}$, $^{52}Cr^{++}$, $^{12}C^{14}N^{+}$, $^{12}C^{12}C^{+}$ and $^{12}C^{13}C^{+}$. The use of a desolvating sample introduction system for solution analysis effectively dries the sample aerosol and makes hydride production negligible (Galy et al., 2001; Young et al., 2002). Non-spectral matrix effects are attributed to changes in analyte sensitivity caused by the abundance of other elements in the sample. A change in analyte sensitivity may be related to a change in instrumental mass bias and many studies have advocated the need for high-purity solutions and concentration-matching of standards and unknowns for bracketing techniques (e.g.

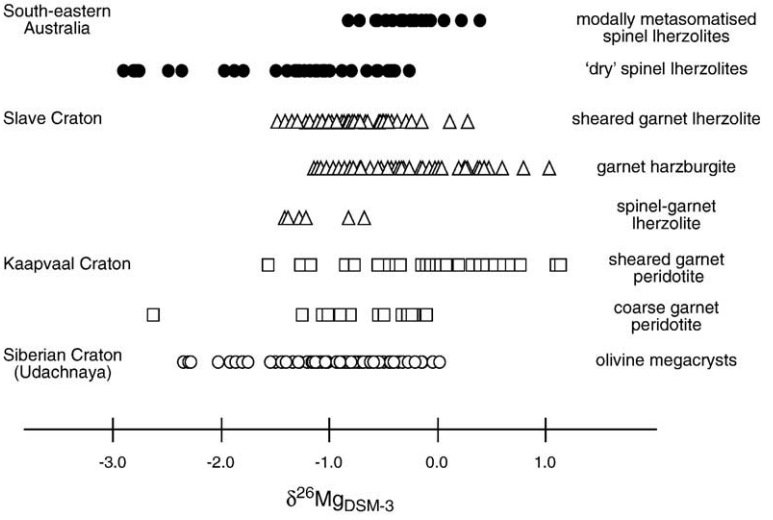

Fig. 11. Range of measured δ^{26}Mg (relative to DSM-3) of olivine from different rock types from the Siberian, Kaapvaal and Slave Cratons and SE Australia.

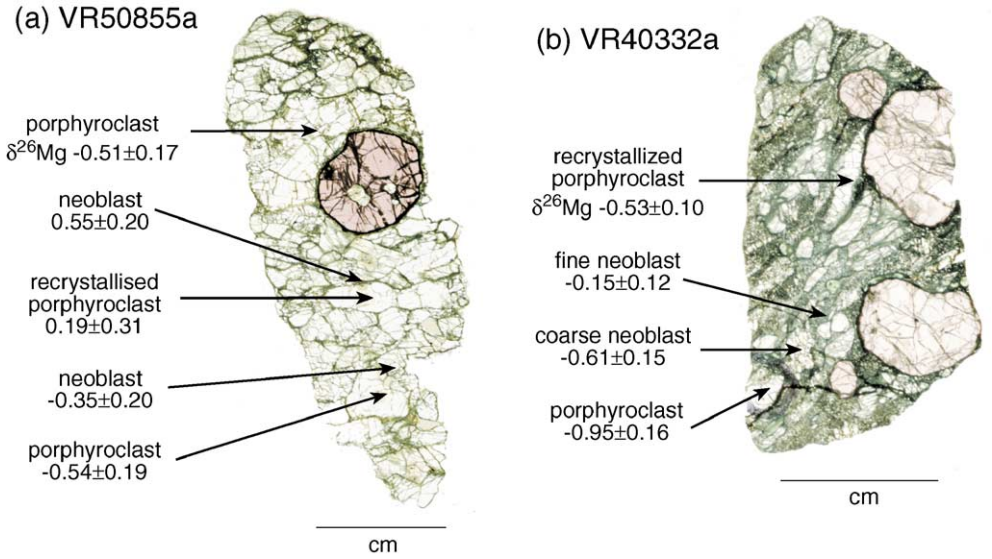

Fig. 12. Variation in δ^{26}Mg in olivine in samples (a) vr50885a and (b) vr40332a.

Mg: Galy et al., 2001; Chang et al., 2003; Fe: Anbar et al., 2000; Kehm et al., 2003; Cu and Zn: Marechal et al., 1999). Although there is consensus that non-spectral matrix effects cannot be ignored there is conflicting evidence for the reproducibility of the effect on mass bias in some isotopic systems. Albarede and Beard (2004) presented data showing the effects of anomalous mass bias in Fe solutions related to the addition of incremental amounts of Mg, Al and La. The disconcerting aspect of the results is the variable magnitude of the shift in Fe isotopic composition with impurity concentration. The worst results were obtained for La, with a positive correlation between ^{56}Fe and La concentration in two analytical sessions and a negative correlation in a third.

There is also some disagreement in the studies that have investigated the effects of contaminant elements on Mg mass fractionation. Most relevant to this study on Mg-rich olivine is the matrix effect related to the addition of Fe. Norman et al. (2004) report the results of measurements made on suite of synthetic olivines (Fo_{70} to Fo_{90}) and showed a shift in instrumental mass bias of +0.06‰ for every 1% decrease in Fo. It was concluded that this was a laser-induced phenomenon as solutions with a similar range in Fe/Mg which showed no variation in isotopic composition. As reported above, we have measured SRM980 Mg solutions spiked with different amounts of IRMM Fe corresponding to a range in olivine compositions with up to 50 mol% of the fayalite end member. The results show there are no consistent relationships between Fe/Mg and deviations from the standard composition, with a maximum range of 0.3‰ in δ^{26}Mg. These solution results agree with those from Galy et al. (2000) and Young et al. (2002), and suggest that the design of the Nu Plasma produces a similar mass bias for each instrument. Young et al. (2002) concluded that there was no measurable shift in ^{25}Mg/^{24}Mg and ^{26}Mg/^{24}Mg for ^{56}Fe/^{24}Mg up to 2.0. These experiments were performed by introducing an Fe solution through a desolvation unit and mixing with ablation products prior to being introduced into the plasma.

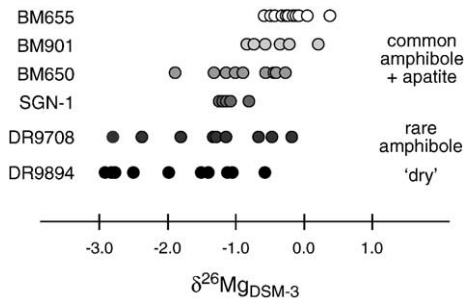

Fig. 13. Range of measured δ^{26}Mg (relative to DSM-3) of olivine from individual samples from SE Australia.

There are many factors put forward to explain matrix-dependent fractionation (e.g. space charge, sample depth, plasma loading, RF power). To explain the disparate results for the solution and laser experiments of Norman et al. (2004), Young and Galy (2004) suggested that fractionation resulted from incomplete transfer after ablation rather than from the ablation process itself. However, the experiments of Young et al. (2002) would point to an ablation process, rather than a plasma

process, being the cause of the mass fractionation. Jackson and Gunther (2003) have shown the importance of particle-size distribution on mass bias, and this is a function of laser energy, repetition rate, and gas composition among other factors.

A series of analyses of ALM-1 was performed in which laser energy was varied to produce a range in signal intensity, to evaluate the effect of plasma loading on mass fractionation. By keeping spot size constant while changing laser energy, a range in energy density was produced, which should give variations in particle-size distribution. The results show no apparent relationship between total Mg signal intensity and the shift in δ^{26}Mg (Fig. 14). These data would indicate that the inverse correlation between Mg signal and δ^{26}Mg reported by Norman et al. (2004) is not a simple dilution or concentration effect. It is apparent that further experiments need to be undertaken to test the results from Norman et al. (2004).

5.2. Mantle processes

The three-isotope plot of the Mg-isotope ratios (Fig. 10), expressed in δ units relative to SRM980, shows that the in situ analyses of olivine grains from the lithospheric mantle lie on the Terrestrial Fractionation Curve determined by Galy et al. (2000). The spread along this trend suggests that the mechanisms controlling the fractionation of Mg isotopes are mass dependent and processes at mantle temperatures are similar to those that have produced the overall range in terrestrial materials.

The range of δ^{26}Mg reported here for olivine grains from mantle-derived peridotites (5‰) covers approximately 3/4 of the total range reported from terrestrial samples; the range of ≥2‰ seen in some single mantle xenoliths represents ca 30% of that range. Much of the terrestrial range is defined by materials produced in low-temperature processes, including organic compounds and sedimentary carbonates (Young and Galy, 2004), whereas our samples have estimated equilibration temperatures (measured by the major-element compositions of coexisting minerals) ranging from 800 to ≥1400 °C. Such large isotopic fractionations are not expected under equilibrium conditions at high temperatures (Urey, 1947); thus the data from the mantle xenoliths clearly imply non-equilibrium processes, and offer new insights into mantle processes at high temperature.

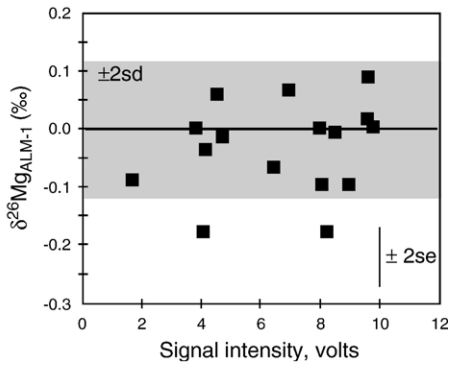

Fig. 14. Plot of δ^{26}Mg versus total Mg signal (laser energy) for laser-ablation analyses of ALM-1.

5.2.1. Sheared high-T peridotites

The high-T sheared peridotite xenoliths offer the best insight into the mechanisms of Mg-isotope fractionation, because the nature and timing of the processes that have affected these rocks are relatively well understood. P–T estimates place most of these xenoliths near the base of the subcontinental lithosphere, in the region from which kimberlite magmas begin their ascent. The cataclastic microstructures of the xenoliths are accompanied by large changes in their bulk composition, including a decrease in Mg/Fe of olivine and other phases, and the introduction of Ca, Al and Fe as shown by increased contents of clinopyroxene and garnet; this metasomatism is ascribed to the passage of large volumes of asthenosphere-derived melts and/or associated fluids (Smith and Boyd, 1987; Griffin et al., 1989; Smith et al., 1993). Neoblastic olivine is typically lower in Mg/Fe and higher in Ca (a measure of T) than relict porphyroblastic olivine. Other porphyroblastic minerals such as garnet show pronounced zoning in major and trace elements, reflecting overgrowths of new material. Modeling of grain-size distributions implies that deformation was actively occurring at the time of eruption (Mercier, 1979), and diffusion modeling of zoning profiles indicates that the metasomatism took place on time scales of 10–10^4 years before eruption (Griffin et al., 1996a). These short time scales are consistent with the preservation of intermineral oxygen-isotope disequilibrium in the closely related polymict peridotite xenoliths (Zheng et al., 2000).

The sheared high-T xenoliths studied here show all of the features typical of this class of mantle peridotite, and show strong correlations between δ^{26}Mg and the microstructural context of each olivine grain. There is a systematic variation between δ^{26}Mg, Ca content (related to temperature) and microstructure of the olivine in sample vr40332a (Fig. 15). The trend to higher δ^{26}Mg in the olivine neoblasts relative to porphyroclasts is also observed in vr50855a. A sheared peridotite from the Kaapvaal Craton (sample LTS98-17, Table 3) shows a

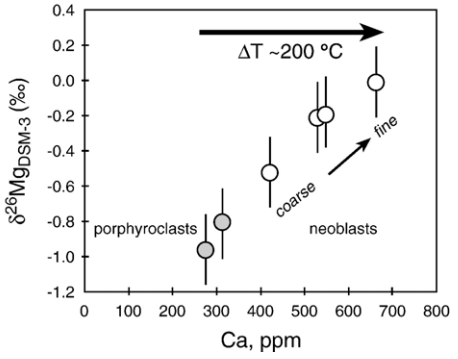

Fig. 15. δ^{26}Mg versus Ca (ppm) in olivine in vr40332a.

range in δ^{26}Mg of 2.7‰. The variation in the δ^{26}Mg of the olivine suggests that parts of these samples have been significantly modified by the passage of metasomatic fluids along distinct pathways; the neoblasts are interpreted as showing the strongest effects of interaction with the fluids. Such modification is likely to be rapid and efficient; Lundstrom (2003) has shown that olivine reacts rapidly with a melt, as Mg diffuses in both directions. Although there is an apparent correlation between temperature (as expressed by Ca in olivine) and δ^{26}Mg in some sheared xenoliths (Fig. 15) we do not regard the isotopic fractionation as temperature-related. Rather, the Ca content of the olivine tracks the degree to which the analysed grains have reacted with the passing melt/fluid.

Galy et al. (2001) assessed the individual effects of the addition of Na, Al and Ca on measured Mg-isotope ratios, and found that Ca produces more significant matrix effects than Fe. Systematic variations were demonstrated for Ca and Al, with increasing positive deviations in δ^{26}Mg (up to 1‰ for Ca; up to 0.4‰ for Al) with increasing Ca/Mg and Al/Mg ratios. It was also observed that at Ca/Mg ratios >0.5, the isobaric interference of doubly charged $^{48}C^{++}$ becomes significant. It is unclear whether the shift in Mg mass bias is due to the $^{48}C^{++}$ interference or simply the matrix effect produced by the presence of Ca. Young et al. (2002) measured $^{44}Ca^{++}$ as a proxy for $^{48}C^{++}$ and reported that shifts in Mg mass bias could be observed when the $^{44}Ca^{++}/^{24}Mg^{+}$ voltage ratio was greater than 0.1%.

All of the olivines analysed in this study have Ca/Mg less than 0.002 and $^{44}Ca^{++}/^{24}Mg^{+}$ voltages are significantly less than 0.1%, with $^{44}Ca^{++}$ in the noise range of the Faraday (<2E−5 V). On this basis it is difficult to conceive that the relationship shown between the Ca content of the olivine and δ^{26}Mg in Fig. 15 is an analytical artifact. Furthermore, the range in Ca contents from the porphyroblasts to the neoblasts (~400 ppm) is less than the difference between the Ca contents of ALM-1 and SC-1 (~670 ppm). If the effect of increasing Ca content even at such a low level is to produce an increase in δ^{26}Mg then a much larger difference, on the order of 1.5‰, would be expected between ALM-1 and SC-1. As this is not the case it is concluded that the interference effects for Ca are negligible in Mg-rich olivine. This is in agreement with the findings of Young et al. (2002) who also concluded that Ca and Ti had insignificant effects for many minerals including Mg-rich olivine and clinopyroxene. They did report that the addition of Na produced an increase in δ^{26}Mg (~0.2‰) but there was no correlation with Na/Mg ratio.

We therefore suggest that the large isotopic differences between the porphyroblast olivine and the neoblasts are the result of physical kinetic isotope fractionation, caused by diffusion along concentration gradients between the fluid and the olivine grains making up the walls of the fluid pathways. Richter et al. (1999, 2003) have demonstrated that diffusion between silicate melts of different compositions produces large isotopic fractionations in Ca, and inferred similar behaviour for Mg. This compositionally driven, diffusion-related fractionation is independent of temperature, and depends on the concentration ratio driving the diffusion. It thus seems probable that diffusion between a percolating melt and a solid phase of markedly different composition could produce equivalent effects. Adopting the diffusion parameters of Richter et al. (2003, Fig. 8), a concentration ratio of 0.2–0.3 ($Mg_{melt}/Mg_{olivine}$) is required to produce the 2–3‰ ranges in δ^{26}Mg seen in the olivine of some of the sheared peridotites. This equates to fluids with 10–15% MgO, well within the range of basaltic melts.

5.2.2. Granular garnet peridotites

The large ranges in δ^{26}Mg over short distances observed in the sheared peridotites (Fig. 12b) are unlikely to be preserved for long times at high temperatures. However, as noted above, these xenoliths essentially have been sampled in statu nascendi, and the evidence of the processes affecting them has been quenched by eruption.

However, relatively large ranges in δ^{26}Mg have also been found in several cratonic garnet peridotite xenoliths with coarse-granular microstructures (Fig. 12a; Table 3), equilibrated at temperatures of 900–1100 °C. Much of this range is expressed as core-to-rim zoning in single olivine grains. By analogy with the high-T sheared peridotites, we interpret this zoning as reflecting the passage of metasomatic fluids, ranging in

composition from hydrous silicate melts to carbonatitic melts (e.g. Grégoire et al., 2002 and references therein). While the olivine and pyroxene grains of such peridotites typically show no major-element zoning, evidence of a metasomatic history commonly is preserved in their garnets (Griffin et al., 1996a, 1999c). The preservation of these isotopic variations within single samples may reflect either slower diffusion at lower temperatures, or a relatively recent metasomatic event. There is increasing evidence that much of the lithospheric mantle beneath the Archean cratons has been metasomatised repeatedly through time (Griffin et al., 1999a; Grégoire et al., 2002; Cousseart et al., 2003), and there is no reason to believe that such metasomatism was not also associated with the eruptive events that brought the xenoliths to the surface.

The proposed mechanism is relevant to understanding the history of single olivine grains hosting sulfides that have been dated by the in situ Re–Os isotope method. The data obtained so far on olivine xenocrysts from Udachnaya show that sulfides interpreted as melt-related (high Re/Os and Pt/Os; Griffin et al., 2002) are hosted by grains with higher δ^{26}Mg, implying that the host olivines have been affected by the metasomatism that introduced the sulfides.

5.2.3. Cryptic and modal metasomatism in spinel peridotites

The effect of modal metasomatism on δMg is evident in the six spinel lherzolites from SE Australia. The samples include assemblages that are 'dry' or least metasomatised (DR9894), cryptically metasomatised (DR9708, SGN-1) and modally metasomatised (amphibole+apatite-bearing; BM650, BM655, BM901) (O'Reilly et al., 1991). Equilibration temperatures range from 800 to 1000 °C. O'Reilly and Griffin (1988) and Griffin et al. (1988) have shown, using chemical and isotopic data, that the metasomatism has occurred in at least three separate episodes, the last of which took place shortly before the Tertiary eruptive event that brought the xenoliths to the surface. Nishio et al. (2004) found a range of 1‰ in δLi in the cpx of four of these xenoliths; ^{7}Li/^{6}Li shows strong correlations with ^{87}Sr/^{86}Sr (positive) and ^{143}Nd/^{144}Nd (negative).

The ranges in olivine composition observed in individual xenoliths, and in the suite as a whole, are less than those seen in the cratonic xenoliths, simply because few off-craton spinel lherzolites are as depleted (in terms of Mg/Fe) as the average cratonic xenolith. There is an overall trend toward higher, and more homogeneous, δ^{26}Mg with increasing degrees of metasomatism. The least metasomatised samples have generally more magnesian olivine, and wide ranges in δ^{26}Mg, whereas the modally metasomatised (amphibole ± apatite-bearing) samples have more Fe-rich olivine and the smallest variation in δMg (Fig. 16). The observed ranges in δ^{26}Mg are much larger than could be explained by the mass-bias effect relating Fo content and δ^{26}Mg proposed by Norman et al. (2004; an increase of 0.02‰ δ^{26}Mg with a decrease of 1% Fo). The within-sample variations provide a further argument against a compositional matrix effect; whereas δ^{26}Mg deviations of up to 2‰ are obtained, the olivine compositions are homogeneous within an uncertainty of ± 0.5 Fo.

By analogy with the high-temperature sheared xenoliths, we interpret these data as showing that the modification of bulk composition by infiltrating metasomatic fluids was accompanied by the physical kinetic isotopic fractionation of Mg by diffusion along large concentration gradients between fluids and their wall rocks. The relatively narrow ranges in δ^{26}Mg in the most strongly metasomatised samples (ca. 1‰) may indicate either that this metasomatism is relatively old, or that the presence of carbonatitic fluids has speeded up isotopic equilibration. The wider ranges in δ^{26}Mg in the least metasomatised samples (up to 2.5‰) may indicate that these samples had escaped metasomatism until shortly before eruption. Clearly, these data indicate the need for detailed studies of larger xenolith suites exhibiting evidence of a range of metasomatic processes. The Li-isotope variations observed in xenoliths from this suite (Nishio et al., 2004) are strongly correlated with other (radiogenic) isotopic measures of metasomatism, and may reflect the same type of kinetic

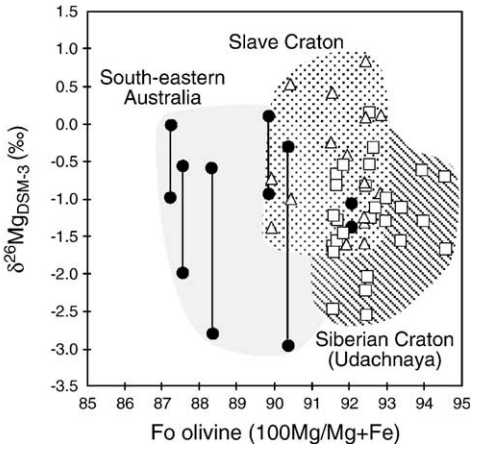

Fig. 16. δ^{26}Mg versus olivine composition (Fo) for samples from the Siberian Craton, Slave Craton and south-eastern Australia. Tie-lines show the range in δ^{26}Mg measured within individual samples showing modal metasomatism.

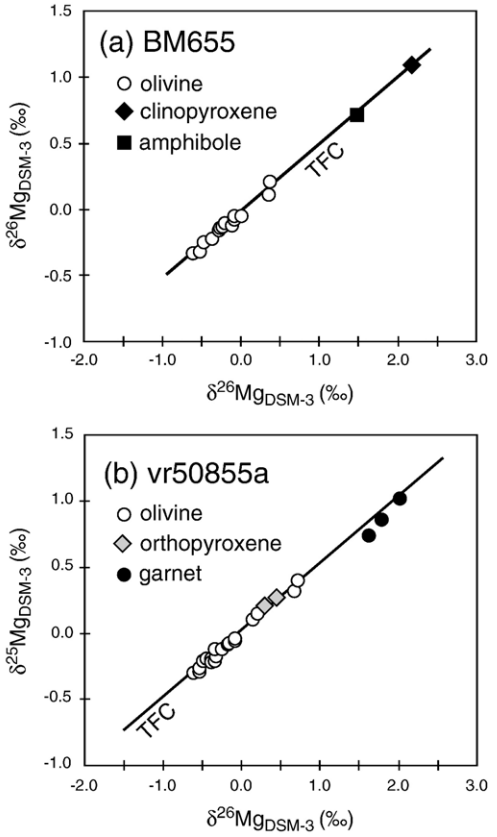

Fig. 17. Magnesium three-isotope plot (relative to DSM-3 Mg standard) showing the fractionation between olivine and coexisting minerals (a) BM655 amphibole-bearing spinel lherzolite, SE Australia; (b) vr50885a garnet harzburgite, Slave Craton. The line labeled TFC is the Terrestrial Fractionation Curve (TFC) from Galy et al. (2000).

isotope fractionation that is shown by the Mg isotopes; Richter et al. (2003) have shown that these effects are even greater for Li than for Mg.

5.2.4. Depletion and refertilisation in the subcontinental lithospheric mantle

Although the data presented here are limited in number and show wide ranges, there is a broad trend observable in both the on-craton and off-craton samples; the most depleted samples in each group tend to have the lowest δ^{26}Mg, while those that have experienced significant metasomatism by asthenosphere-derived melts and/or fluids have higher δ^{26}Mg. The depletion process (*s.l.*) has involved the extraction of mafic to ultramafic melts from a fertile protolith; the metasomatic processes have involved the re-introduction of such melts and associated fluids into the SCLM. The observed variations suggest that the melt-extraction process has involved an isotopic fractionation of Mg, with the melts having higher δ^{26}Mg than the source rock, leaving the resulting residue with a lower δ^{26}Mg. The combination of these two processes may be sufficient to explain the observed range in the δ^{26}Mg of mantle olivine, ranging from the products of (multiple?) depletion events at the light end, to the compositions of primitive mantle melts at the high end.

This scenario implies that melt extraction is a non-equilibrium process, at least in detail. It predicts that a recently depleted residue, sampled as a xenolith, might show a core-to-rim zoning toward lower δ^{26}Mg in single olivine grains, in contrast to the trends observed in our limited sample. As noted above, there is considerable evidence that the cratonic lithospheric mantle has been extensively refertilised over time. If our samples are representative, the lowest δ^{26}Mg values reported here may represent maximum values for the highly depleted SCLM, while the heaviest values might approximate the δ^{26}Mg of the asthenosphere.

5.2.5. Intermineral fractionation

Preliminary Mg-isotope measurements on clinopyroxene and amphibole in BM650 and BM901 provide additional evidence that links the shift to heavier δ^{26}Mg in the olivine with metasomatism. Both clinopyroxene and amphibole have markedly higher δMg than coexisting olivine (Fig. 17). However, a number of matrix effect issues need to be addressed to validate these results. Some of these have been investigated using synthetic mineral solutions, prepared by adding Ca, Fe and minor elements Cr, Al to the SRM980 solution in mole proportions equivalent to clinopyroxene, amphibole, orthopyroxene and garnet. The results are shown in Fig. 18 and the effect of the addition of Fe for the synthetic olivine compositions has already been discussed. The synthetic clinopyroxene and amphibole compositions are shifted to slightly higher δMg values

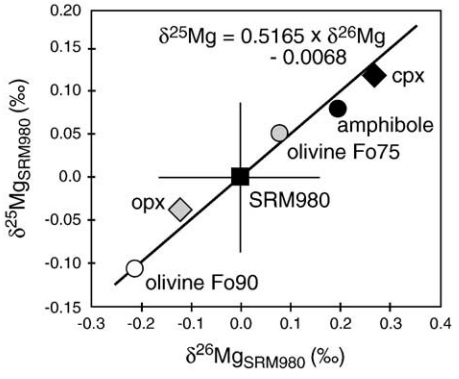

Fig. 18. Magnesium three-isotope plot (relative to SRM980 Mg standard) of synthetic mineral solutions.

but, like the synthetic orthopyroxene, are within uncertainty (±2sd) of the unspiked SRM980. This indicates that any matrix effects brought about by the addition of Ca up to Ca/Mg=1 are not sufficient to produce the intermineral fractionation observed between olivine and clinopyroxene in the xenoliths. The synthetic garnet is also shifted to higher δMg relative to SRM980 but again it would not appear that the presence of Al in the sample matrix is the cause of the difference in δMg measured between olivine and garnet in sample vr50885a.

The fractionation of Mg isotopes between peridotite phases in this study shows a number of similarities and differences to those reported for Fe isotopes (Zhu et al., 2002). As with Mg isotopes, the olivine was shown to have systematically lighter Fe than coexisting clinopyroxene in the three samples studied by Zhu et al., with differences in ε^{57}Fe of 1.8 to 3.7 between the two minerals. One of the three samples had been modally metasomatised and the amphibole contained significantly heavier Fe than the coexisting olivine and clinopyroxene. In contrast to the Mg isotopes there was no observed fractionation of Fe isotopes between orthopyroxene and clinopyroxene. Zhu et al. (2002) concluded that the fractionation between olivine and pyroxenes indicated equilibrium partitioning and cited the equilibrium distribution of oxygen isotopes (Mattey et al., 1994) as supporting this view.

Young and Galy (2004) found that Mg in olivine is 1‰ lighter than coexisting clinopyroxene. To explain the Fe isotope results for the amphibole, Zhu et al. (2002) suggested that because it was a metasomatic product it might not be in equilibrium with the olivine and pyroxenes. Consequently the large fractionation of Fe isotopes between amphibole and the other minerals was interpreted to indicate the possible importance of kinetic processes in isotope fractionation at high temperature. Further detailed studies of Fe, Mg, Ca and O isotopes in metasomatised peridotites clearly will be required to document and understand these fractionations in a larger variety of rock types.

6. Conclusions

- The in situ measurement of Mg isotopes in olivine by laser-ablation MC-ICPMS provides a robust analytical method to investigate isotopic variations in mantle peridotites.
- A range of 5‰ δ^{26}Mg has been found in olivine from several suites of xenoliths and xenocrysts, representing the lithospheric mantle beneath Archean cratons and Phanerozoic fold belts.
- Melt extraction (depletion) leads to isotopically lighter Mg in the residue, and there is a consistent shift to heavier isotopic compositions related to subsequent metasomatism and melt infiltration.
- Variations of up to 2.6‰ δ^{26}Mg occur within individual peridotite xenoliths and the in situ technique allows these variations to be interpreted in a microstructural context.
- The magnitude and scale of the variations within samples suggest that non-equilibrium processes are important; the most likely process for producing these variations is physical kinetic isotope fractionation related to diffusion of Mg between high-Mg olivine and low-Mg melts/fluids. On a three-isotope plot the olivine data spread along the Terrestrial Fractionation Curve. Therefore both equilibrium and disequilibrium processes produce isotopic fractionations that fall on this curve.
- Preliminary data on coexisting minerals indicate disequilibrium or partial re-equilibration; further studies clearly are needed to investigate these effects in more detail.

Acknowledgements

The authors are delighted to take part in this homage to Keith O'Nions, and want to thank him for his inspiration and generosity over more years than he would like to remember. Good times have included shared postdoc experiences in Oslo and dating eclogites at Lamont, and He-isotope games and accompanying lab parties at Oxford. Keith's role in the development of the Nu Plasma MC-ICPMS has opened many new research opportunities for all of us, and he didn't even object (very much) to us putting Os solutions through his prototype instrument. The ideas in this paper have been presented at the 12th Goldschmidt Conference, Davos, the 8th International Kimberlite Conference and the 17th Australian Geological Convention. Comments received at these meetings have improved our understanding of mass-dependent fractionation. The original manuscript also was improved following detailed reviews by A. Galy and C. Lundstrom, as well as comments from the Special Editor, Gideon Henderson. Dr. Slava Spetsius is thanked for supplying the Udachnaya olivine xenocrysts. This is contribution No. 408 from the ARC National Key Centre for the Geochemical Evolution and Metallogeny of Continents (http:/www.els.mq.edu.au/GEMOC). **[SG]**

References

Albarede, F., Beard, B.L., 2004. Analytical methods for non-traditional isotopes. In: Johnson, C.M., Beard, B.L., Albarede, F. (Eds.), Geochemistry of Non-Traditional Stable Isotopes, Reviews in Mineralogy and Geochemistry vol 55. Mineralogical Society of America, Washington, pp. 113–152.

Anbar, A.D., Roe, J.E., Barling, J., Nealson, K.H., 2000. Nonbiological fractionation of iron isotopes. Science 288, 126–128.

Carder, E.A., Galy, A., Elderfield, H.E., 2004. The magnesium isotopic composition of oceanic water masses, 14th Annual Goldschmidt Conf, Copenhagen, DK. Geochim. Cosmochim. Acta 68 (supplement 1), A324.

Chang, V.T.-C., Makishima, A., Belshaw, N., O'Nions, K., 2003. Purification of Mg from low-Mg biogenic carbonates for isotope ratio determination using multiple collector ICP-MS. J. Anal. At. Spectrom. 18, 296–301.

Cousseart, N., Gregoire, M., Mercier, J.C., Bell, D.R., Demaiffe, D., le Roux, Andre, L., 2003. The origin of clinopyroxene in the cratonic mantle. Extended Abstract (Abstract No. FLA_0383), 8th International Kimberlite Conference.

Freedman, P.A., 2002. Mass bias in ICP mass spectrometers. Geochim. Cosmochim Acta 66, A245. (Abstracts of the 12th Annual Goldschmidt Conference).

Galy, A., Young, E.D., Ash, R.D., O'Nions, R.K., 2000. The formation of chondrules at high gas pressures in the Solar Nebula. Science 290, 1751–1753.

Galy, A., Belshaw, N.S., Halicz, L., O'Nions, R.K., 2001. High-precision measurement of magnesium isotopes by multiple-collector inductively coupled plasma mass spectrometry. Int. J. Mass. Spectrom. 208, 89–98.

Galy, A., Bar-Matthews, M., Halicz, L., O'Nions, R.K., 2002. Mg isotopic composition of carbonate: insight from speleothem formation. Earth Planet. Sci. Lett. 6248, 1–11.

Galy, A., Yoffe, O., Janney, P.E., Williams, R.W., Cloquet, C., Alard, O., Halicz, L., Wadhwa, M., Hutcheon, I.D., Ramon, E., Carignan, J., 2003. Magnesium isotope heterogeneity of the isotopic standard SRM980 and new reference materials for magnesium-isotope-ratio measurements. J. Anal. At. Spectrom. 18, 1352–1356.

Grégoire, M., Bell, D.R., Le Roux, A.P., 2002. Trace element geochemistry of phlogopite-rich mafic mantle xenoliths: their classification and their relationship to phlogopite-bearing peridotites and kimberlites revisited. Contrib. Mineral. Petrol. 142, 603–625.

Griffin, W.L., Wass, S.Y., Hollis, J.D., 1984. Ultramafic xenoliths from Bullenmerri and Gnotuk maars, Victoria, Australia: petrology of a subcontinental crust–mantle transition. J. Petrol. 25, 53–87.

Griffin, W.L., O'Reilly, S.Y., Stabel, A., 1988. Mantle metasomatism beneath Victoria, Australia: II. Isotope geochemistry of Cr-diopside lherzolites and Al-augite pyroxenites. Geochim. Cosmochim. Acta. 52, 449–459.

Griffin, W.L., Smith, D., Boyd, F.R., Cousens, D.R., Ryan, C.G., Sie, S.H., Suter, G.F., 1989. Trace element zoning in garnets from sheared mantle xenoliths. Geochim. Cosmochim. Acta. 53, 561–567.

Griffin, W.L., Smith, D., Ryan, C.G., O'Reilly, S.Y., Win, T.T., 1996a. Trace element zoning in mantle minerals: metasomatism and thermal events in the upper mantle. Can. Mineral. 34, 1179–1193.

Griffin, W.L., Kaminsky, F.V., Ryan, C.G., O'Reilly, S.Y., Win, T.T., Ilupin, I.P., 1996b. Thermal state and composition of the lithospheric mantle beneath the Daldyn kimberlite field, Yakutia. Tectonophysics 262, 19–33.

Griffin, W.L., Doyle, B.J., Ryan, C.G., Pearson, N.J., O'Reilly, S.Y., Natapov, L., Kivi, K., Kretschmar, R., Ward, J., 1998. Lithosphere structure and mantle terranes: Slave Craton, Canada. The 7th International Kimberlite Conference Proceeding, J.B. Dawson vol. 1. , pp. 299–306.

Griffin, W.L., O'Reilly, S.Y., Ryan, C.G., 1999a. The composition and origin of subcontinental lithospheric mantle. In: Fei, Y., Bertka, C.M., Mysen, B.O. (Eds.), Mantle Petrology: Field Observations and High-pressure Experimentation: A Tribute to Francis R. (Joe) Boyd, Geochem. Soc. Spec. Publ. vol. 6. The Geochemical Society, Houston, pp. 13–45.

Griffin, W.L., Doyle, B.J., Ryan, C.G., Pearson, N.J., O'Reilly, S.Y., Davies, R., Kivi, K., Van Achterbergh, E., Natapov, L.M., 1999b. Layered mantle lithosphere in the Lac de Gras area, Slave Craton: composition, structure and origin. J. Petrol. 40, 705–727.

Griffin, W.L., Shee, S.R., Ryan, C.G., Win, T.T., Wyatt, B.A., 1999. Harzburgite to lherzolite and back again: metasomatic processes in ultramafic xenoliths from the Wesselton kimberlite, Kimberley, South Africa. Contrib. Mineral. Petrol. 134, 232–250.

Griffin, W.L., Spetsius, Z.V., Pearson, N.J., O'Reilly, S.Y., 2002. In situ Re–Os analysis of sulfide inclusions in kimberlitic olivine: new constraints on depletion events in the Siberian lithospheric mantle. Geochem. Geophys. Geosyst. 3, 1–25.

Griffin, W.L., O'Reilly, S.Y., Natapov, L.M., Ryan, C.G., 2003a. The evolution of lithospheric mantle beneath the Kalahari Craton and its margins. Lithos 71, 215–242.

Griffin, W.L., O'Reilly, S.Y., Abe, N., Aulbach, S., Davies, R.M., Pearson, N.J., Doyle, B.J., Kivi, K., 2003b. The origin and evolution of Archean lithospheric mantle. Precambr. Res. 127, 19–41.

Griffin, W.L., Graham, S., O'Reilly, S.Y., Pearson, N.J., 2004. Lithospheric evolution beneath the Kaapvaal Craton: Re–Os systematics of sulfides in mantle-derived peridotites. Chem. Geol. 208, 89–118.

Jackson, S.E., Gunther, D., 2003. The nature and sources of laser-induced isotopic fractionation in laser ablation-multi collector-inductively coupled plasma-mass spectrometry. J. Anal. At. Spectrom. 18, 205–212.

Kehm, K., Hauri, E.H., Alexander, C.M.O'D., Carlson, R.W., 2003. High precision iron isotope measurements of meteoritic material by cold plasma ICP-MS. Geochim. Cosmochim. Acta 67, 2879–2891.

Lundstrom, C.C., 2003. An experimental investigation of the diffusive infiltration of alkalis into partially molten peridotite: implications for mantle melting processes. Geochem. Geophys. Geosyst. 4 (9), 8614 (doi: 10.1029/2001GC00024).

Marechal, C.N., Telouk, P., Albarede, F., 1999. Precise analysis of copper and zinc isotopes by plasma-source mass spectrometry. Chem. Geol. 156, 251–273.

Matsumoto, T., Honda, M., McDougall, I., O'Reilly, S.Y., Norman, M., Yaxley, G., 2000. Noble gases in pyroxenites and metasomatised peridotites from the Newer Volcanics, southeastern Australia: implications for mantle metasomatism. Chem. Geol. 168, 49–73.

Mattey, D., Lowry, D., MacPherson, C., 1994. Oxygen isotope composition of mantle peridotite. Earth Planet. Sci. Lett. 128, 231–241.

Mercier, J.-C.C., 1979. Peridotite xenoliths and the dynamics of kimberlite intrusion. In: Boyd, F.R., Meyer, H.O.A. (Eds.), The Mantle Sample: Inclusions in Kimberlites and Other Volcanics. American Geophysical Union, Washington, D.C., pp. 197–212.

Nishio, Y., Nakai, S., Yamamoto, J., Sumino, H., Matsumoto, T., Prikhod'ko, V.S., Arai, S., 2004. Lithium isotope systematics of the mantle-derived xenoliths: implications for EM1 origin. Earth Plan. Sci. Lett. 217, 245–261.

Norman, M., McCulloch, M., O'Neill, H., Brandon, A., 2004. Magnesium isotopes in the Earth, Moon, Mars and pallasite parent body: high precision analysis of olivine by laser ablation multi-collector ICPMS. Lunar Planet. Sci. XXXV, 1447.

O'Reilly, S.Y., Griffin, W.L., 1988. Mantle metasomatism beneath Victoria, Australia I: metasomatic processes in Cr-diopside lherzolites. Geochim. Cosmochim. Acta 52, 433–437.

O'Reilly, S.Y., Griffin, W.L., Ryan, C.G., 1991. Residence of trace elements in metasomatized spinel lherzolite xenoliths: a proton-microprobe study. Contrib. Mineral. Petrol. 109, 98–113.

Pearson, N.J., Griffin, W.L., Doyle, B.J., O'Reilly, S.Y., van Achterbergh, E., Kivi, K., 1999. Xenoliths from kimberlite pipes of the Lac de Gras area, Slave Craton, Canada. In: Gurney, J., Gurney, J., Pascoe, M., Richardson, S. (Eds.), Proc. 7th Int. Kimb. Conf. Red Roof Design, Cape Town, pp. 644–663.

Pearson, N.J., Alard, O., Griffin, W.L., Jackson, S.E., O'Reilly, S.Y., 2002. In situ measurement of Re–Os isotopes in mantle sulfides by laser ablation multicollector-inductively coupled plasma mass spectrometry: analytical methods and preliminary results. Geochim. Cosmochim. Acta 66, 1037–1050.

Powell, W., Zhang, M., O'Reilly, S.Y., Tiepolo, M., 2004. Mantle amphibole trace element and isotopic signatures trace multiple metasomatic episodes in lithospheric mantle, western Victoria, Australia. Lithos 75, 141–171.

Richter, F.M., Liang, Y., Davis, A.M., 1999. Isotope fractionation by diffusion in molten oxides. Geochim. Cosmochim. Acta 63, 2853–2861.

Richter, F.M., Davis, A.M., DePaolo, D.J., Watson, E.B., 2003. Isotope fractionation by chemical diffusion between molten basalt and rhyolite. Geochim. Cosmochim. Acta 67, 3905–3923.

Smith, D., Boyd, F.R., 1987. Compositional heterogeneities in a high-temperature lherzolite nodule and implications for mantle processes. In: Nixon, P.H. (Ed.), Mantle Xenoliths. J. Wiley and Sons, pp. 551–561.

Smith, D., Griffin, W.L., Ryan, C.G., 1993. Compositional evolution of high-temperature sheared lherzolite PHN1611. Geochim. Cosmochim. Acta 57, 605–613.

Urey, H.C., 1947. The thermodynamic properties of isotopic substances. J. Chem. Sic., 562–581.

Wombacher, F., Risenhauer, A., Bock, B., Fietzke, J., 2004. Magnesium stable isotope compositions of reference solutions, 14th Annual Goldschmidt Conf, Copenhagen, DK. Geochim. Cosmochim. Acta 68 (supplement 1), A324.

Young, E.D., Galy, A., 2004. The isotope geochemistry and cosmochemistry of magnesium. In: Johnson, C.M., Beard, B.L., Albarede, F. (Eds.), Geochemistry of Non-Traditional Stable Isotopes, Reviews in Mineralogy and Geochemistry vol 55. Mineralogical Society of America, Washington, pp. 197–230.

Young, E.D., Ash, R.D., Galy, A., Belshaw, N.S., 2002. Mg isotope heterogeneity in the Allende meteorite measured by UV laser ablation-MC-ICPMS and comparisons with O isotopes. Geochim. Cosmochim. Acta. 66, 683–698.

Zheng, J.-F., Mattey, D., Grassineau, N., Lowry, D., Brownless, M., Gurney, J.J., Menzies, M.A., 2000. Recent fluid processes in the Kaapvaal Craton, South Africa: coupled oxygen isotope and trace element disequilibrium in polymict peridotites. Earth Planet. Sci. Lett. 176, 57–72.

Zhu, X.K., Guo, Y., Williams, R.J.P., O'Nions, R.K., Matthews, A., Belshaw, N.S., Canters, R.W., de Waal, E.C., Wester, U., Burgess, B.K., Salvato, B., 2002. Mass fractionation processes of transition metal isotopes. Earth Planet. Sci. Lett. 200, 47–62.